ON THE INVERSE KINEMATICS OF A FRAGMENT OF PROTEIN BACKBONE

Guanfeng Liu[†], R.J. Milgram[‡], A. Dhanik[†], and J.C. Latombe[†]
[†] *Department of Computer Science, Stanford University*
[‡] *Department of Mathematics, Stanford University*
{liugf,ankur,latombe}@cs.stanford.edu and milgram@math.stanford.edu

Abstract This paper studies the structure of the inverse kinematics (IK) map of a fragment of protein backbone with 6 torsional degrees of freedom. The images (critical sets) of the singularities of the orientation and position maps are computed for a slightly idealized kinematic model. They yield a decomposition of $SO(3)$ and $\mathcal{R}^3$ into open regions where the number of IK solutions is constant. A proof of the existence of at least one 16-solution cell in $\mathcal{R}^3 \times SO(3)$ is given and one such case is shown.

Keywords: Protein backbone, inverse kinematics, critical sets.

1. Introduction

A protein (Creighton, 1993) is a sequence of amino-acids connected by peptide bonds. It is often modeled as a serial linkage, the *backbone*, with short side-chains. Each amino-acid contributes three atoms – N, C_α, and C – and two torsional degrees of freedom (dofs) to the backbone (Fig. 1). These dofs correspond to the dihedral angles ϕ and ψ around the N – C_α and the C_α – C bonds. The inverse kinematics of the backbone is of considerable interest in biology (Coutsias et al, 2004).

Let F be a backbone fragment with 6 dihedral angles ϕ and ψ, and f be its forward kinematics. It is well-known that the number of solutions of the inverse kinematics (IK) map f^{-1} has 16 as an upper bound, but it has often been questioned whether this bound is tight (Coutsias et al, 2004). Available algorithms only compute these solutions for *given* poses of the moving frame T of F. Here, we study the *global* structure of f^{-1} over the entire 6-D manifold of poses of T in $\mathcal{R}^3 \times SO(3)$. The images of the singularities of f are the *critical* poses, which, according to the Morse-Sard theorem, decompose the noncritical part of the image into open regions, such that in each region E, $f^{-1}(x)$ for each $x \in E$ contains the same number of points. These decompositions of the 6-D manifold can be very complex, so we study the position map p and an orientation map ρ separately. It turns out ρ is quite easy to understand and the original question reduces to studying the projection to $\mathcal{R}^3$ from

the inverse images of ρ. Given the frame associated to T, the set of configurations that give the frame is either a copy of $(S^1)^3$ or a copy of the disjoint union $(S^1)^3 \sqcup (S^1)^3$. Focusing on these $(S^1)^3$, we can compute p^{-1} more efficiently and we find regions with 16 inverse image points. This result is reasonable since a 6-dof protein fragment does not satisfy any of the conditions under which the IK of a 6-dof serial linkage has less than 16 solutions (Mavroidis and Roth, 1994).

2. Kinematic Model of a Protein Fragment

Let F be a 6-dof fragment of a protein backbone as illustrated in Fig. 1. The coordinates of F are the 3 dihedral angles ϕ_i around the bonds $\mathrm{N}^i\text{–}\mathrm{C}^i_\alpha$, and the 3 dihedral angles ψ_i around the bonds $\mathrm{C}^i_\alpha\text{–}\mathrm{C}^i$. For convenience, we rename ϕ_i by θ_{2i-2} and ψ_i by θ_{2i-1}, so each conformation of F is specified by a 6-tuple $\theta = (\theta_1, \ldots, \theta_6) \in (S^1)^6$.

We represent F by a kinematically equivalent sequence of 3 identical units, each made of two perpendicular links, a "long" one of length ℓ_2 and a "short" one of length ℓ_1, as shown in Fig. 2. We number the links $1, 2, \ldots, 6$, so that each link $2i-1$ is a long link and each link $2i$ is a short link. Angle θ_{2i-1} rotates short link $2i$ about long link $2i-1$. So, each short link moves in a plane perpendicular to the preceding long link. Angle θ_{2i} rotates the long link $2i+1$ about an axis parallel to long link $2i-1$ and passing through the extremity of short link $2i$. Link $2i+1$ makes the constant angle $\alpha = 19$ degrees with the plane perpendicular to link $2i-1$. Finally, we add a long link 7 to F. This is the link associated with the moving frame T.

We summarize these remarks and put them into a mathematical setting as follows. Set

$$R_i = \begin{bmatrix} \cos(\theta_i) & -\sin(\theta_i) & 0 \\ \sin(\theta_i) & \cos(\theta_i) & 0 \\ 0 & 0 & 1 \end{bmatrix}, \qquad L = \begin{bmatrix} -\sin(\alpha) & 0 & \cos(\alpha) \\ 0 & -1 & 0 \\ \cos(\alpha) & 0 & \sin(\alpha) \end{bmatrix},$$

where $\alpha \sim .105556\pi$ is fixed and $L^T = L^{-1} = L$. Then, the orientations of the frames are given by

$$O_1 = I_{3\times 3}, \quad O_{2i} = O_{2i-1}R_{2i-1}, \quad O_{2i+1} = O_{2i}R_{2i}L,$$

and f is the composition of p and ρ with

$$p : (S^1)^6 \to \mathcal{R}^3, \quad \theta \to (R_{1;2}L + R_{1;2}LR_{3;4}L)v_1 + (R_1 + R_{1;2}LR_3 + R_{1;2}LR_{3;4}LR_5)v_2, \quad (1)$$

$$\rho : (S^1)^6 \to SO(3), \quad \theta \to R_{1;2}LR_{3;4}LR_{5;6}L, \quad (2)$$

where $R_{i;j} = R_iR_j$, $v_1 = [0,\ 0,\ \ell_2]^T$, and $v_2 = [\ell_1,\ 0,\ 0]^T$.

This paper studies the structure of the inverse kinematics $f^{-1} = (p, \rho)^{-1}$. Noticing that for any $(X, R) \in \mathcal{R}^3 \times SO(3)$,

$$(p, \rho)^{-1}(X, R) = p^{-1}(X) \cap \rho^{-1}(R),$$

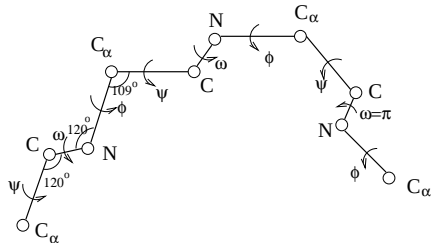

Figure 1. 6-dof fragment

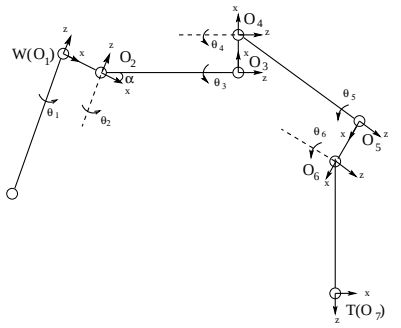

Figure 2. Equivalent model

we proceed in two steps. First, we derive the inverse orientation map $\rho^{-1} : SO(3) \rightarrow (S^1)^6$ and show that in general $\rho^{-1}(R)$ is the disjoint union of two 3-D tori $\mathcal{M}_1$ and $\mathcal{M}_2$. Next, we compute $p_k^{-1}(X)$, where p_k, $k \in 1, 2$, is the map p with its domain restricted to $\mathcal{M}_k$.

3. Inverse Orientation Map

Reduction. In Eq. (2) only the sums $\theta_{2i-1}+\theta_{2i}$ appear. So, we write $\tau_i = \theta_{2i-1} + \theta_{2i}$, $i = 1,\ 2,\ 3$, and $\tau = (\tau_1, \tau_2, \tau_3)$. As θ runs over $(S^1)^6$, τ runs over the 3-D torus $(S^1)^3$, and ρ factors as composition

$$\rho \ = \ \hat{\rho} \circ (+) : (S^1)^6 \rightarrow (S^1)^3 \rightarrow SO(3)$$

where $\hat{\rho} : (S^1)^3 \rightarrow SO(3),\ \tau \rightarrow R_{\tau_1} L R_{\tau_2} L R_{\tau_3} L$. R_{τ_i} is the rotation of angle τ_i around the z axis. Given $R \in SO(3)$, the values of $\hat{\rho}^{-1}(R)$ are the solutions of $\hat{\rho}(\tau) := R_{\tau_1} L R_{\tau_2} L R_{\tau_3} L \ = \ R$, which is equivalent to:

$$\hat{\rho}(\tau) L := R_{\tau_1} L R_{\tau_2} L R_{\tau_3} \ = \ RL. \tag{3}$$

Since $\hat{\rho}(\tau)L$ defines the frame on the z-axis, (which is fixed by R_{τ_3}, we further reduce Eq. (3) by eliminating the variable τ_3. To do this, we define $A_z : SO(3) \rightarrow S^2,\ \ R \rightarrow Rz$, where $z = [0,\ 0,\ 1]^T$ and S^2 denotes the unit 2-D sphere. Since $A_z(R_{\tau_3}) = z$, applying A_z to both sides of Eq. (3) yields:

$$A_z(\hat{\rho}(\tau) L) := R_{\tau_1} L R_{\tau_2} L z \ = \ RLz \tag{4}$$

where $R_{\tau_1} L R_{\tau_2} L$ defines the orientation of the z-axis of frame 6 in W. We can solve this equation for (τ_1, τ_2). The value of τ_3 is then uniquely determined by:

$$R_{\tau_3} = (R_{\tau_1} L R_{\tau_2} L)^T RL. \tag{5}$$

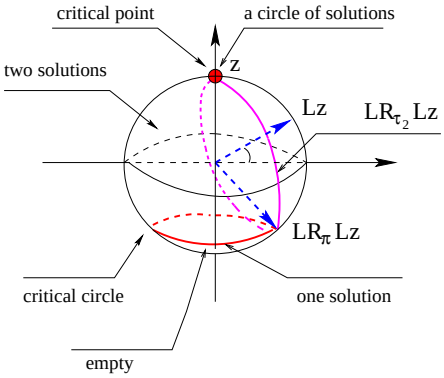

Figure 3. Critical set of η

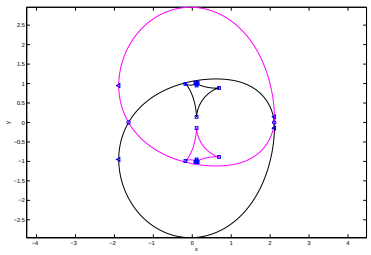

Figure 4. The discriminant curve $\mathcal{X}_d$ computed with $\gamma = \pi$ and $d = -0.32$.

To each solution $\tau = (\tau_1, \tau_2, \tau_3)$ of Eqs. (4) and (5) corresponds a set of values of $\theta = (\theta_1, ..., \theta_6)$ such that $\theta_{2i-1} + \theta_{2i} = \tau_i$ for $i = 1,\ 2,\ 3$. This set is a 3-D torus $(S^1)^3$.

Singular set. The singularities of $\hat{\rho}$ are the points in $(S^1)^3$ where the 3×3 Jacobian matrix $J\hat{\rho}$ has rank less than 3. When working with Lie groups, the Jacobian is $(d\hat{\rho})\hat{\rho}^{-1}$. This gives a map to the Lie algebra. The Lie algebra of $SO(3)$ is 3-dimensional and a change of basis gives $J\hat{\rho} = [z,\ R_{\tau_1}Lz,\ R_{\tau_1}LR_{\tau_2}Lz]$, z as above. $J\hat{\rho}$ has at least rank 2. It has has rank exactly 2 if and only if: $det(J\hat{\rho}) = \sin(\tau_2)\cos(\alpha) = 0$. As $\cos(\alpha) \neq 0$, the singular set of $\hat{\rho}$ is $\{\tau \mid \tau_2 = 0\} \cup \{\tau \mid \tau_2 = \pi\}$.

Critical set and number of solutions. The quotient map $\eta : (S^1)^3 \to SO(3) \to S^2$ that appears in the left-hand side of Eq. (4), has the same singular set as $\hat{\rho}$. The critical set of η – i.e., the image of $\{\tau \mid \tau_2 = 0\} \cup \{\tau \mid \tau_2 = \pi\}$ – is the union of $C_1 = R_{\tau_1}R_{\tau_3}z = z$ and $C_2 = R_{\tau_1}LR_\pi LR_{\tau_3}z = R_{\tau_1}LR_\pi Lz$ for all $\tau_1 \in S^1$. C_1 is the point that corresponds to the situation where the z-axes of W and frame 6 are parallel. Indeed, when $\tau_2 = 0$, the z-axis of frame 6 is parallel to the z-axis of W for any value of τ_1. On the other hand, $R_{\tau_1}LR_\pi Lz = [(\sin(2\alpha)\cos(\tau_1),\ \sin(2\alpha)\sin(\tau_1),\ -\cos(2\alpha)]^T$, so C_2 is the circle perpendicular to the z-axis and passing through the point $LR_\pi Lz$. See Fig. 3.

The inverse map η^{-1}, hence $\hat{\rho}^{-1}$, has a constant structure in C_1, C_2, and in each of the two open subsets of S^2 bounded by C_1 and C_2. We notice that: $L(LR_{\tau_2}Lz) = [\cos(\alpha)\cos(\tau_2),\ \cos(\alpha)\sin(\tau_2),\ \sin(\alpha)]^T$. So, $LR_{\tau_2}Lz$ is a circle perpendicular to Lz contained in the subset of S^2 be-

tween C_1 and C_2, except at $\tau_2 = 0$ and $\tau_2 = \pi$ where it coincides with C_1 and C_2, respectively (Fig. 3). For any fixed $\tau_1 \in S^1$, the set $R_{\tau_1} L R_{\tau_2} L z$ is the circle obtained by rotating $L R_{\tau_2} L z$ by τ_1 around the z axis. Thus, for every point s in the region between C_1 and C_2, $R_{\tau_1} L R_{\tau_2} L z$ contains s for two distinct values of τ_1. We conclude that η^{-1} has two values (τ_1^k, τ_2^k), $k = 1,\ 2$. In C_1, $s = z$ and $\eta^{-1}(s) = \{(\tau_1, 0) \mid \tau_1 \in S^1\}$. For any $s \in C_2$, $\eta^{-1}(s)$ has a single value of the form (τ_1, π). Elsewhere $\eta^{-1}(s)$ is empty.

Corresponding to each value (τ_1, τ_2) of $\eta^{-1}(s)$ there is a unique value of τ_3 given by Eq. (5), hence a single value of $\hat{\rho}^{-1}(R)$. Thus, as we initialize an orientation $R \in SO(3)$ not in the critical sets C_1 and C_2, $\rho^{-1}(R)$ is the disjoint union of two 3-D tori, written $\mathcal{M}_k$, $k = 1, 2$.

4. Inverse Position Map

Restriction to $\mathcal{M}_k$. We now study $p_k^{-1}(X)$, where $X \in \mathcal{R}^3$ and p_k, $k \in 1, 2$, is the position map p with its domain restricted to $\mathcal{M}_k$. Since $\theta_{2j-1} + \theta_{2j}$, $j = 1,\ 2,\ 3$, are constant on $\mathcal{M}_k$ and equal to τ_j^k, each point on $\mathcal{M}_k$ is uniquely defined by the values of θ_1, θ_3, and θ_5. Eq.(1) yields:

$$p_k : (S^1)^3 \to \mathcal{R}^3, \quad (\theta_1, \theta_3, \theta_5) \to v_{0,k} + (R_1 + R_{\tau_1^k} L R_3 + R_{\tau_1^k} L R_{\tau_2^k} L R_5) v_2$$

where $v_{0,k} = (R_{\tau_1^k} L + R_{\tau_1^k} L R_{\tau_2^k} L) v_1$ is a constant vector and $\{R_1 v_2\}$, $\{R_{\tau_1^k} L R_3 v_2\}$, and $\{R_{\tau_1^k} L R_{\tau_2^k} L R_5 v_2\}$ are constant circles of radius ℓ_1 contained in three different planes.

Computing $p_k^{-1}(X)$ amounts to solving the equation:

$$X' = \hat{p}_k(-\theta_2, \theta_3, \theta_5) := R_{-2} v_2 + L R_3 v_2 + L R_{\tau_2^k} L R_5 v_2, \tag{6}$$

where $X' = R_{\tau_1^k}^T (X - v_{0,k})$ and R_{-2} is the rotation of $-\theta_2$ around z.

Critical set. Here we directly determine the critical positions X' where the number of solutions of $\hat{p}_k$ changes. We rewrite Eq. (6) as:

$$X' - r(w) = q(t, u), \tag{7}$$

where we rename the variables as $t = -\theta_2$, $u = \theta_3$, $w = \theta_5$, and $\gamma = \tau_2^k$. $X' - r(w)$ is a unit circle centered at X' and $q(t, u)$ spans a quartic surface Q in $\mathcal{R}^3$. Q is the Minkowski sum of two circles, so it is bounded and connected. Eq. 7 can be solved by computing the intersections between $X' - r(w)$ and the coss-section curve of Q by the plane containing $X' - r(w)$. We compute $r(w) = \hat{x} c_w + \hat{y} s_w$. $\hat{x} = [s_\alpha^2 c_\gamma + c_\alpha^2,\ s_\gamma s_\alpha,\ s_\alpha c_\alpha (1 - c_\gamma)]^T$ and $\hat{y} = [-s_\alpha s_\gamma,\quad c_\gamma,\ c_\alpha s_\gamma]^T$ form an orthonormal basis for the plane

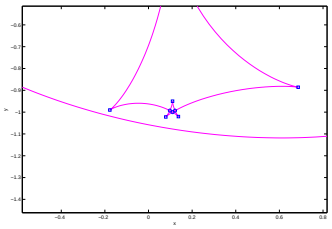

Figure 5. Zoom on a portion of $\mathcal{X}_d$ in Fig. 4. The centers of the small squares and the small circles are cusp points and self-intersection points, respectively.

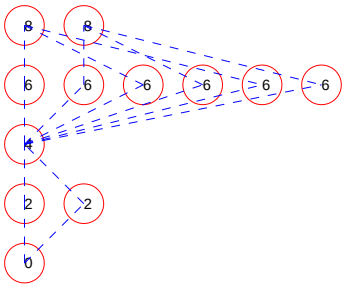

Figure 6. The planar graph determined by the discriminant curve of Fig. 4. The number of solutions is shown in each node.

containing the circle $r(w)$. Setting $\hat{z} = \hat{x} \times \hat{y}$, the equation of the plane containing $X' - r(w)$ is:

$$\hat{z}^T q \quad = \quad d \tag{8}$$

where $d = \hat{z}^T X'$. We let P_d denote the plane defined by this equation. When X' spans $\mathcal{R}^3$, P_d translates, but its orientation remains constant.

On the other hand, we can easily compute:

$$q(t,u) \quad = \quad [c_t - s_\alpha c_u, \quad s_t - s_u, \quad c_\alpha c_u]^T . \tag{9}$$

By replacing q by this expression in Eq. (8), we get the equation of the cross-section Q_d of Q by P_d in terms of (t,u):

$$c_{(u-\gamma)} + K(\gamma) s_{(t+\beta)} \quad = \quad \frac{d}{c_\alpha} \tag{10}$$

where $c_\beta = -\frac{s_\gamma}{K(\gamma)}$, $s_\beta = \frac{s_\alpha(1-c_\gamma)}{K(\gamma)}$, and $K(\gamma) = \sqrt{s_\gamma^2 + s_\alpha^2(1-c_\gamma)^2}$.

The number of intersection points in $Q_d \cap (X' - r(w))$ varies as X' runs over $\mathcal{R}^3$. The X' such that the circle is tangent to Q_d form the critical set $\mathcal{X} \subset \mathcal{R}^3$ of $\hat{p}_k$. Let $d_{\min}$ and $d_{\max}$ be the extreme values of d between which the plane $\hat{z}^T q = d$ and Q intersect. For any $d \in [d_{min}, d_{max}]$, the values of X' such that $X' - r(w)$ lies in the plane P_d and is tangent to Q_d form a curve $\mathcal{X}_d$ called the *discriminant curve* at d. The union of the discriminant curves for d in $[d_{\min}, d_{\max}]$ is the critical surface $\mathcal{X}$ of $\hat{p}_k$. Fig. 4 shows a discriminant curve, with several cusp and self-intersection points. An animation of both the cross-section of Q and the corresponding discriminant curve when d varies is available at `www.stanford.edu/~phwu1/curve` when $\gamma = \pi$.

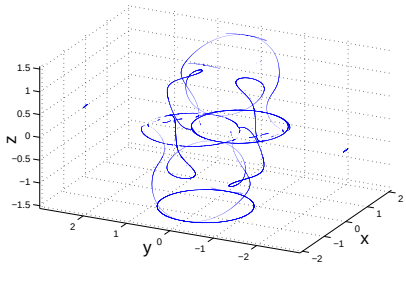

Figure 7. The cusp curves when $\gamma = \pi$.

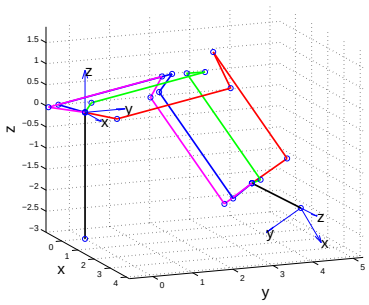

Figure 8. Four of the 16 solutions.

Decomposition of $\mathcal{R}^3$ into regions. The surface $\mathcal{X}$ decomposes $\mathcal{R}^3$ into open 3-D regions such that the number of solutions of the inverse position map is constant over each one. We first compute the decomposition of a plane P_d by $\mathcal{X}_d$. Next, we partition $[d_{min}, d_{max}]$ into smaller open intervals, such that over each such interval the discriminant curves $\mathcal{X}_d$ are equivalent. We get the decomposition of $\mathcal{R}^3$ by "stacking" the decompositions in the successive intervals.

Decomposition of P_d: We sweep a line L parallel to the y-axis across the plane P_d from left to right to construct a set S of sub-regions and their adjacency relations. S is initialized to the empty set. During the sweep, whenever L crosses a cusp point, a self-intersection point, or a vertical tangency point, sub-regions are added to S and the adjacency relation is updated. When the sweep is completed, adjacent sub-regions in S not separated by $\mathcal{X}_d$ are merged to form the decomposition of P_d. The outcome is a planar *graph* in which the nodes are the computed regions and the edges represent the adjacency relation. The number of solutions of the inverse position map varies by 2 at each crossing of a region boundary. We compute cusp and self-intersection points numerically by approximating the discriminant curve by line segments. Fig. 6 shows the graph computed from the discriminant curve shown in Fig. 4. An animation of the discriminant curve and the corresponding graph when d varies is available at `www.stanford.edu/~phwu1/curve` when $\gamma = \pi$.

Decomposition of $\mathcal{R}^3$: As d varies from d_{min} to d_{max}, the planar graph in P_d changes only at a finite number of *critical* values of d, which we denote d_i, $i = 1, ..., m$. Over each open interval (d_i, d_{i+1}), $i = 0, ..., m$, with $d_0 = d_{min}$ and $d_{m+1} = d_{max}$, the discriminant curves are equivalent and the planar graph remains constant. Let G_i be the planar graph in

interval (d_i, d_{i+1}). The decomposition of $\mathcal{R}^3$ is obtained by merging every pair of regions from G_i and G_{i+1}, for all $i = 0, ..., m$, that are adjacent, but not separated by $\mathcal{X}$. The corresponding nodes of the planar graphs are also merged to obtain the graph of the decomposition of $\mathcal{R}^3$.

The 2-D surface $\mathcal{X}$ is made of smooth patches separated by cusp and self-intersection curves. The cusp (resp. self-intersection) curves are the locus $\mathcal{X}^{\text{cusp}}$ (resp. $\mathcal{X}^{\text{self}}$) of all the cusp (self-intersction) points of the discriminant curves $\mathcal{X}_d$ when d varies. The critical values of d are contributed by $\mathcal{X}\backslash(\mathcal{X}^{\text{cusp}} \cup \mathcal{X}^{\text{self}})$, $\mathcal{X}^{\text{cusp}}$, and $\mathcal{X}^{\text{self}}$. For lack of space, we do not describe their computation here. Fig. 7 shows $\mathcal{X}^{\text{cusp}}$ for $\gamma = \pi$.

5. Existence of a 16-Solution Cell

Theorem 1 *There exists a nonempty open region in $\mathcal{R}^3 \times SO(3)$ such that for all (X, R) in this region, $(p, \rho)^{-1}(X, R)$ contains 16 points.*

Proof: Consider first an orientation $R_0 \in SO(3)$ that lies in the critical circle C_2. $\rho^{-1}(R_0)$ is a copy of $(S^1)^3$. There is a nonempty open region $E_0 \subset C_2$ such that for all R in E_0, $p(\rho^{-1}(R))$ has an open region U so that $p^{-1}(X)$ contains 8 points for $X \in U$ (see Fig. 6). Let R' be a noncritical orientation that is close to E_0. Then $\rho^{-1}(R')$ is a disjoint union of two 3-D tori $\mathcal{M}_k$, $k = 1, 2$. For each p_k, there exists a nonempty open region E_k with 8 inverse image points. Moreover, for R' sufficiently close to E_0, $E = E_1 \cap E_2$ is nonempty. Then $(p, \rho)^{-1}(X, R')$ has 16 solutions for all $X \in E$. ■

Using the idea in the proof, we constructed the following pose (X, R) of T:

$$X = \begin{bmatrix} 1.9760 \\ 4.5809 \\ -2.2402 \end{bmatrix} \quad \text{and} \quad R = \begin{bmatrix} 0.6742 & -0.3715 & -0.6383 \\ 0.2378 & -0.7091 & 0.6638 \\ -0.6992 & -0.5993 & -0.3897 \end{bmatrix},$$

such that $(p, \rho)^{-1}(X, R)$ contains 16 solutions (for a fragment in which $\ell_1 = 1$ and $\ell_2 = 3$). Four of them are shown in Fig. 8. (It is easily seen that the existence of 16-solution cell is independent of the link lengths as long as the short links all have the same length.)

Acknowledgements: This research was funded by NSF grant DMS-0443939.

References

Coutsias, E.A., Seok, C, Jacobson, M.P., and Dill, K.A. (2004), A kinematic view of loop closure. *J. Comp. Chem.*, 25:510–528.

Creighton, T.E. (1993), *Proteins : Structures and molecular properties*. W. H. Freeman and Company, New York, 2nd edition.

Mavroidis, C., and Roth, B. (1994), Structural Parameters which reduce the number of manipulator configurations. *J. Mech. Design, Trans. ASME*, vol. 116, pp. 3–10.